Tensile strength of carbon nanotubes under realistic temperature and strain rate

Chenyu Wei,[1,2] Kyeongjae Cho,[1] and Deepak Srivastava[2]
[1]*Department of Mechanical Engineering, Stanford University, California 94305*
[2]*NASA Ames Research Center, MS T229-1, Moffett Field, California 94035*
(Received 23 September 2002; revised manuscript received 26 December 2002; published 17 March 2003)

A transition state theory based predictive model is developed for the tensile failure of carbon nanotubes (CNT's). We show that the tensile yield strain has linear dependence on the activation energy and the temperature, and has a logarithmic dependence on the strain rate. Based on the parameters fitted from strain rate and temperature-dependent simulations within a wide range of molecular-dynamics time scales, the model predicts that a defect-free micrometer long single-wall nanotube at 300 K, stretched with a strain rate of 1%/h, yields at about $9\pm1\%$ tensile strain for small diameter CNT's, and about 2–3 % higher for larger diameter CNT's. This is in good agreement with recent experimental findings.

DOI: 10.1103/PhysRevB.67.115407 PACS number(s): 61.48.+c, 62.20.Fe

Since their discovery in 1990s,[1] carbon nanotubes (CNT's) have been found to have exceptional mechanical properties with Young's modulus as high as 1 TPa, and also novel electronic properties. Applications of CNT's as nanofibers or building blocks for nanodevices have been proposed and are investigated in many current studies. The efficiency of the reinforcement of nanocomposites with CNT nanofibers or mechanical stabilities of CNT based nanodevices will be largely dependent on the intrinsic mechanical properties of CNT's. This includes not only the modulus of CNT's which is a measure of the stiffness and strength at small strains, but also the yielding of CNT's at large strains.

Earlier atomistic molecular-dynamics (MD) simulations performed at very high strain rates (limited by time scale of the phenomenon that can be simulated in MD) show tensile yield strain of CNT's to be as high as 30%.[2,3] Whereas, recent experiments report much smaller tensile yield strain in a variety of scenario. Walters *et al.*[4] have reported a yield strain of 5.8% on single-walled CNT (SWCNT) ropes. Yu *et al.*[5] have reported a similar value of maximum 5.3% strain for yielding at room temperature, and have measured strain for yielding of multiwalled CNT's (MWCNT) (Ref.6) to be as high as 12%.

The yielding or failure of CNT's is mainly dependent on the activation and propagation of defects, such as Stone-Wales (SW) bond rotation or graphitic (sp^2) to sp^3 diamondlike bonding transitions at the location of collapse. The former has been mainly formed on tensile strained CNT's,[7–9] whereas the latter has been mainly observed on axially compressed CNT's.[10,11] Previous theoretical and numerical simulation studies have shown that, under large tensile strain, SW bond rotations result in the formation of pentagon-heptagon pair (5775) defects on the nanotubes (Fig. 1),[7–9] which are energetically favorable at tensile strain larger than 5%.[8,9] However, the large energy barriers (of about 8–9 eV) to the formation of SW bond rotations in static calculations[7] do not readily explain the experimentally measured low tensile strength of SWCNT ropes or MWCNT's. On the other hand, the high strain rates used in the earlier MD simulations, limited by the time scales accessible to MD methods, are generally of the order of picosecond^{-1} or faster. This is also unrealistic because the experimental strain rates are of the order of min^{-1} or slower. A clear deficiency thus exists in a direct comparison of earlier MD simulated tensile strength with what is measured in experiments.

One way to accelerate the kinetic processes in MD simulations is to increase the temperature. The transition time for an activated process in that case is typically given by the Arrhenius relation $t=(1/\nu)e^{E_\nu/k_BT}$, where E_ν is the activation energy and ν is the effective vibration or attempt frequency of the transition. At high temperatures, a larger kinetic energy increases the rate of the process to overcome the barriers and the transition time is shortened. This increases the efficiency of the MD simulations of activated processed. In this study, a transition state theory (TST) based predictive

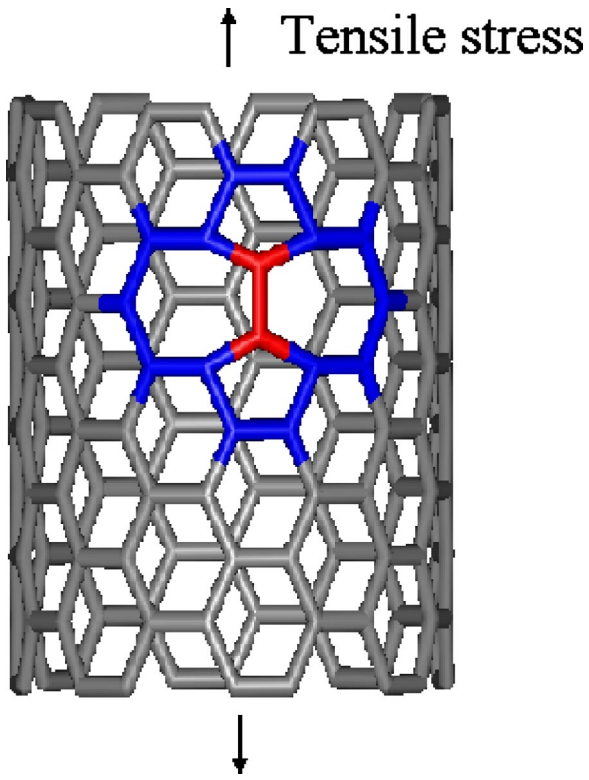

FIG. 1. A Stone-Wales bond rotation defect shown on an armchair CNT under tension.

model for tensile yielding of SWCNT's has been developed. Based on the parameters fitted from extensive MD simulations at different temperatures and strain rates, we are able to predict tensile failure of micrometer long SWCNT's at experimentally feasible strain rates and temperatures.

MD simulations of SWCNT's involve solution of Hamilton's equations of motion for the full system, under different thermodynamic ensembles. In our MD study, Langevin friction force scheme[13] is used to control the kinetic temperature and time step is kept fixed at 0.5 fs. Tersoff-Brenner potential is used for C-C interactions,[14,15] which can describe bond formation and breaking dynamics in the simulated system, and which was parametrized from graphite, diamond, and hydrocarbon molecular systems. Tersoff-Brenner potential has been used to study the mechanical properties of CNT's, such as Young's modulus[16,17] and the activation energy of Stone-Wales bond rotation defects,[8] and provides reliable results as compared with the more accurate tight-binding[7,18] or *ab initio* density-functional theory based methods.[9,19]

The MD simulations of tensile strain involve continuous stretching of nanotubes by moving the end atoms under tensile strain, and letting the nanotube relax during the dynamics at constant temperatures and strain rates. A 0.25% tensile strain is applied in a single MD step and the strain rate is maintained by the time interval allowed for the relaxation of the system before the next 0.25% strain is applied. A 60 Å long (10,0) nanotube with 600 atoms is used for the simulation studies (with 40 end atoms at each end used for applying the strain), and the CNT is strained at rates varying within four orders of magnitude (from 10^{-6} ps^{-1} to 10^{-2} ps^{-1}) and at temperatures ranging from 300 K to 2400 K. The simulations are CPU time intensive. For example, a change of strain of 0.25% was followed by a MD relaxation of 5×10^6 time steps for a strain rate of 10^{-6}/ps. The atomic configurations and energies of the CNT's are monitored and recorded during the simulations, and it is possible to observe yielding of nanotubes within the simulated strain rates and temperatures.

The strain energy per atom for different temperatures and strain rates, as a function of tensile strain, is plotted in Fig. 2(a). The abrupt deviation of the strain energy from the elastic behavior at high strain values (and we define such strain as the yield strain or failure strain) is found to be triggered off by the appearance of SW bond rotations. This is shown, for example, in Fig. 2(b) (lower panel) by plotting a trajectory of the change in the strain energy of the (10,0) CNT as a function of MD evolution time close to yielding. The formation of a SW defect in a nantube or graphene lattice typically involves a bond rotation with breaking of two existing C-C bonds and the formation of two new C-C bonds. For a SW bond rotation within a strained CNT, this can be monitored by tracking the changes in the neighbors of each C atom during the dynamics. For a single SW bond rotation, four C atoms change one of their three neighbors. The number of C atoms with their one, two, or three neighbors changed during the yielding trajectory is plotted in Fig. 2(b) (upper panel). The correlation between the energetics with the changes in the number of neighbors show that the yielding of the CNT is onset by bond rotations. Multiple bond

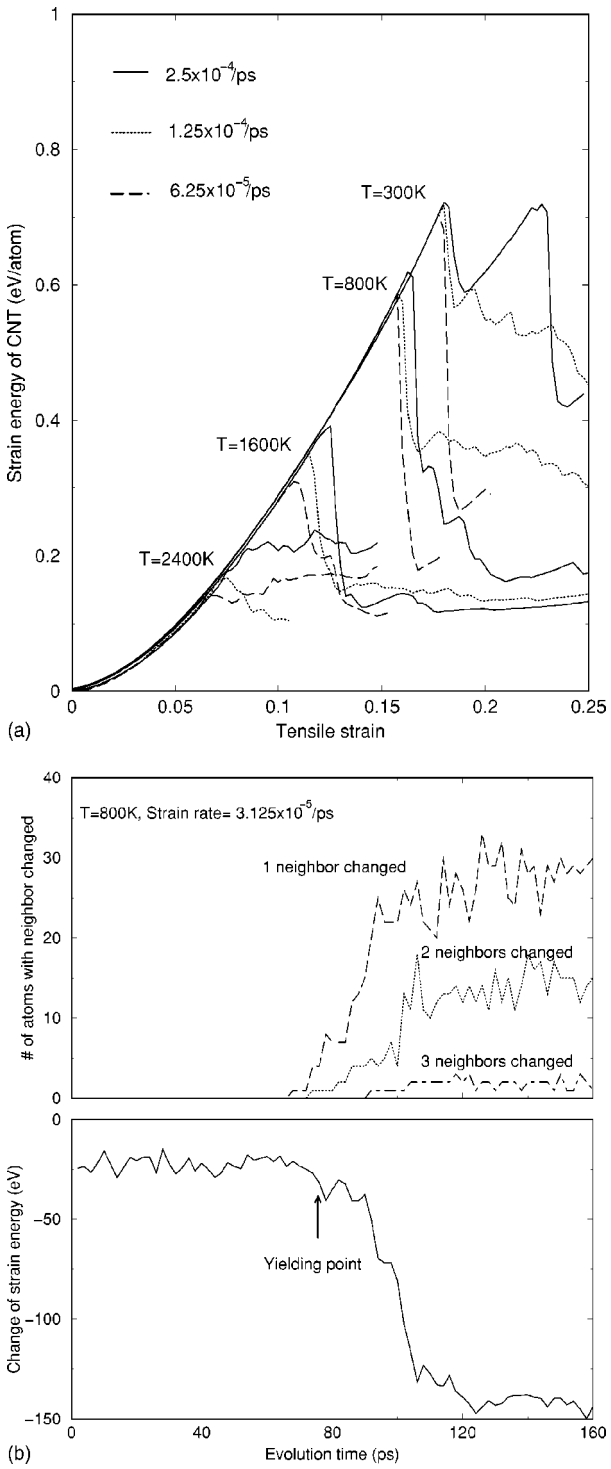

FIG. 2. (a) The strain energy per atom as a function of tensile strain for CNT(10,0) at different temperatures and strain rates. The strain at which the abrupt derivation of strain energy from elastic behavior is defined as yield strain. (b) (upper panel) The number of atoms involved in bond rotations as a function of evolution time are plotted. The atoms with 1, 2, or 3 neighbors changed involve in 1, 2, or 3 bond rotations, respectively. The label for the *X* axis is same as the one for the lower panel of Fig. 2(b). (lower panel) The change of the strain energy of a (10,0) CNT as a function of evolution time close to yielding. It is seen that the yielding of CNT is onset by bond rotation defects.

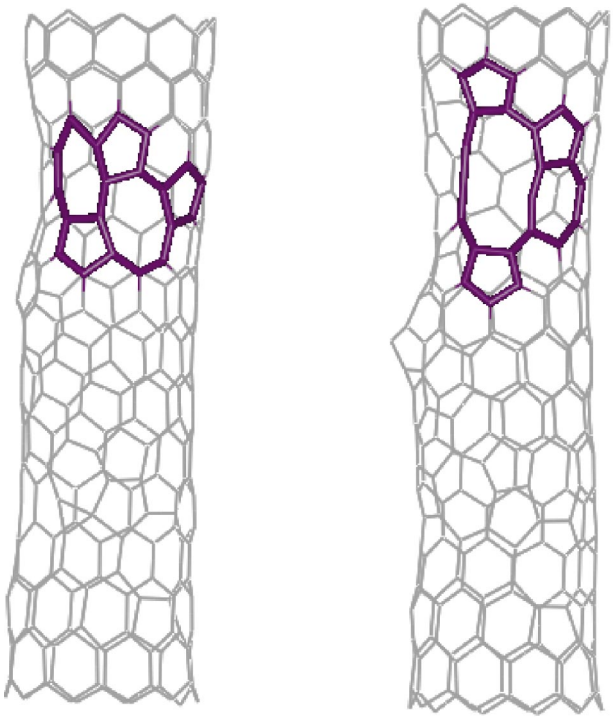

FIG. 3. The atomic configurations of the 11.5% strained CNT (10,0) near its yield strain at $T=1600$ K (shown is the section of the 60 Å CNT). Left: a group of pentagon and heptagon centered by an octagon which are resulted from several SW rotations in the connected region. Right: the followed of the start of the breaking of the CNT (10,0). Defects are marked in dark.

rotations leading to multiple SW defects also occur, and this is accompanied by the eventual necking and breaking of the nanotubes. The example data shown in Fig. 2(b) is at $T=800$ K with a strain rate of 3×10^{-5} ps^{-1}. The trajectories at other temperatures and strain rates show similar results. Shown in Fig. 3 is the atomic configurations of a 11.5% strained CNT (10,0) near its yield strain at $T=1600$ K. The configuration on the left shows a group of pentagon and heptagon centered by an octagon that results from several SW rotation in the connected region; and the one on right shows the start of breaking of the CNT (10,0).

The yield strain as a function of different strain rates and temperatures, within a wide range, is shown in Fig. 4(a). The figure shows that the yield strain decreases at higher temperatures and at slower strain rates. The yield strain depends linearly on temperature and logarithmically on strain rate. The slope of the linear dependence increases with temperature. This indicates that the Arrhenius behavior as a function of temperature is valid. The tensile yielding of nanotubes thus can be described by a theory of activated processes, i.e., the transition of the system from the initial pre-yielding state to the final post-yielding state occurs through a series of activated processes with an effective barrier defining the characteristics of the whole phenomenon. In the following analysis, we develop a TST based model and show that the data of the yield strain, limited to within MD time scales and temperatures, enables the parametrization of the model at all experimentally feasible temperatures and strain rates as well.

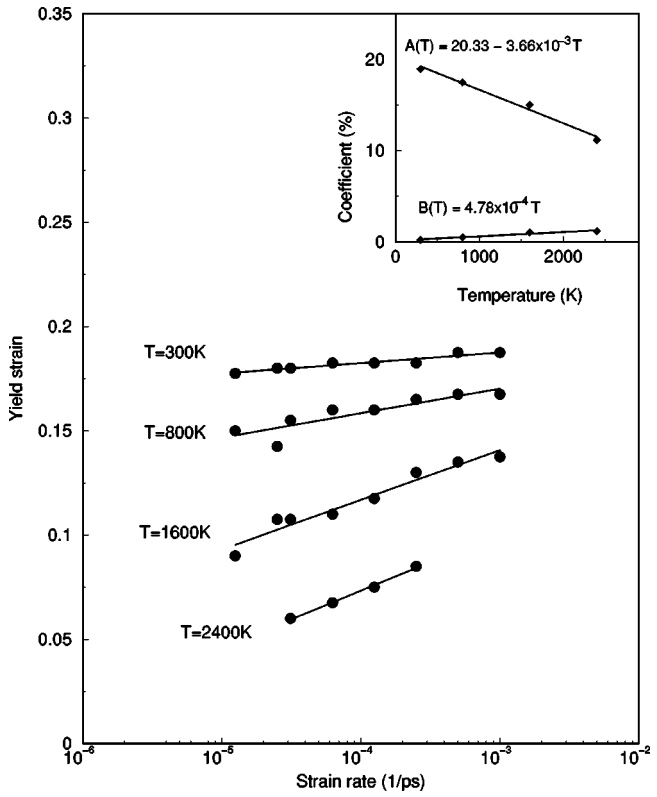

FIG. 4. The tensile yield strain of (10,0) CNT as a function of strain rate at different temperatures, which is seen to decreased with high temperature and slow strain rate. Inset: $A(T)$ and $B(T)$ defined in Eq. (5) as functions of T. The linear behaviors show that the transition state theory based model described in Eq. (4) is valid.

For example, the predicted yielding of a micron long SWCNT at 300 K, strained at a rate of 1%/h, compares very well with the recent experimental observations.

According to the Eyring's theory, the Arrhenius formula for a strained system can be modified as[12]

$$t=\frac{1}{n_{site}}\frac{1}{\nu}e^{(E_\nu-VK\epsilon)/k_BT}, \tag{1}$$

where t is transition time, ϵ is local strain, n_{site} is number of sites available for state transition, K is force constant, and V is the activation volume. Thus, by rewriting Eq. (1) the strain rate required for a transition at a certain strain is

$$\frac{1}{\dot{\epsilon}}=\frac{1}{n_{site}}\frac{1}{\dot{\epsilon}_0}e^{(E_\nu-VK\epsilon)/k_BT}, \tag{2}$$

where $\dot{\epsilon}$ is strain rate and $\dot{\epsilon}_0$ is the intrinsic strain rate, a constant related with vibration or attempt frequency. The yield strain as a function of temperature and strain rate, thus, can be expressed by inverting Eq. (2) as

$$\epsilon_Y=\frac{E_\nu}{VK}+\frac{k_BT}{VK}\ln\frac{\dot{\epsilon}}{n_{site}\dot{\epsilon}_0}. \tag{3}$$

For nanotubes under tensile strain, we have observed that the yielding process induces a sequence of SW type bond

rotations within the connected local regions. These transitions lead to a collective kinetic activation mechanism of the failure of CNT's strained beyond elastic limit. The combined rate for N multiple transitions thus can be of the form $1/Nt$, where $1/t$ is the rate for a single transition and for simplicity we have assumed that the rate for each successive transition can be expressed by an averaged value of $1/t$. An averaged effective activation energy $\overline{E_\nu}$ for the multiprocess thus replaces E_ν for the single process, and Eq. (3), can be modified as:

$$\epsilon_Y = \frac{\overline{E_\nu}}{VK} + \frac{k_B T}{VK} \ln \frac{N\dot{\epsilon}}{n_{site}\dot{\epsilon}_0}. \tag{4}$$

In the following analysis, we show that the TST based model derived in Eq. (4) is fully supported by the MD simulation results. This is accomplished by rewriting Eq. (4) as

$$\epsilon_Y = \left[\frac{\overline{E_\nu}}{VK} - \frac{k_B T}{VK} \ln\left(\frac{\dot{\epsilon}_0 n_{site}}{N\Delta\epsilon_{step}} \right) \right] + \frac{k_B T}{VK} \ln \frac{\dot{\epsilon}}{\Delta\epsilon_{step}}$$

$$= A(T) + B(T) \ln \frac{\dot{\epsilon}}{\Delta\epsilon_{step}}, \tag{5}$$

where $A(T) = (\overline{E_\nu}/VK) - (k_B T/VK)\ln(n_{site}\dot{\epsilon}_0/N\Delta\epsilon_{step})$ and $B(T) = k_B T/VK$ are identified as the intercept and slope, respectively, of the linear behavior shown in Fig. 4(a), and $\Delta\epsilon_{step}$ is the change of strain at each step used in simulations. The functional dependence of $A(T)$ and $B(T)$ over the entire temperature range is obtained by comparing the expression in Eq. (5) to the simulation data at different temperatures. The linear dependence of both $A(T)$ and $B(T)$ on the temperature shown in the inset, Fig. 4(b), indicates that the TST based derived model is valid for the yielding of the strained CNT's in the entire range. From the dependence of $B(T)$ on T, we get $VK = 18.04$ eV. For one-dimensional CNT's, with Young's modulus giving the force constant to be 1 TPa, the activation volume comes out to be 2.88 Å^3. This corresponds to a typical atomic volume of a carbon atom within a nanotube. The comparison of the coefficients in $A(T)$ gives $\overline{E_\nu}/VK = 0.20$ and $(k_B/VK)\ln(n_{site}\dot{\epsilon}_0/N\Delta\epsilon_{step}) = 3.66\times10^{-5}$. These values correspond to the average kinetic activation energy $\overline{E_\nu}$ of 3.6 eV for the SW bond rotations triggering the failure of the nanotube. In our simulations, with $n_{site} \approx 600$ and $\Delta\epsilon_{step} = 0.0025$ or 0.25%, $\dot{\epsilon}_0/N$ comes out to be about 8×10^{-3} ps^{-1}. ϵ_Y is not dependent on $\Delta\epsilon_{step}$ as the effects cancel out in $A(T)$ and $B(T)$. There is always a possibility for the inverse transitions which have rates scaled as $e^{-2VK\epsilon/k_B T}\dot{\epsilon}$, and are omitted as $(VK\epsilon/k_B T) \gg 1$ in our study. The good fitting of the MD data to Eq. (4) shows that the above model is valid, and moreover the parameters such as activation volume and intrinsic strain rate can be obtained.

The yield strain of the CNT's, under tensile stress with experimentally feasible strain rates, can be estimated or *predicted from the above model*. For example, at $T = 300$ K and at a strain rate of about 1%/h, the yield strain for a 6 nm long

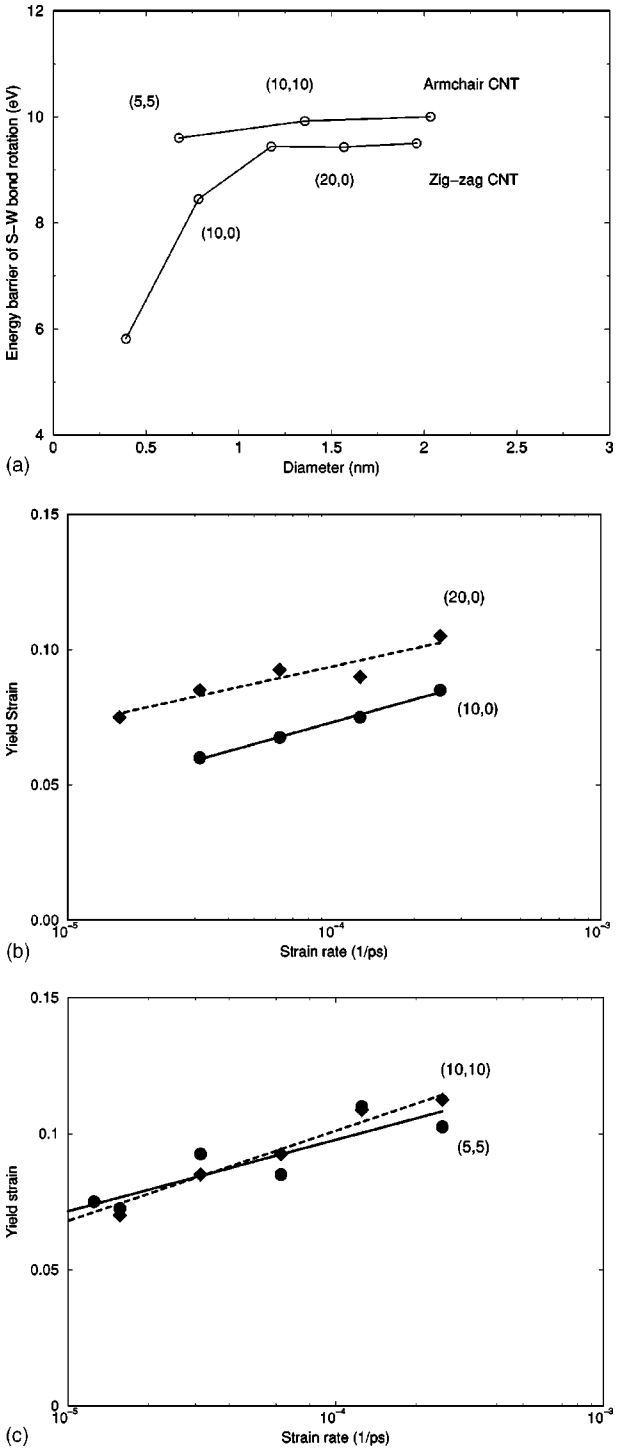

FIG. 5. (a) The static in-plane activation energy of Stone-Wales bond rotations as a function of diameters for zigzag and armchair CNTs, using Tersoff-Brenner potentials. Small diameter zigzag tube such as (10,0) has lower activation energy compared to larger diameter tubes. (b) and (c) The yield strain of (10,0) (circle and solid line), (20,0) (diamond and dashed line), (5,5) (circle and solid line) and (10,10) (diamond and dashed line) CNTs as a function of strain rate at $T = 2400$ K. The lines are linear fits of the yield strain to the logarithm of the strain rate, for the simulation data shown in solid circles or diamonds. The difference in the static activation energy on these tubes as shown in (a) is reflected in the yield strain.

(10,0) CNT comes out to be about $11\pm1\%$ as according to $\epsilon_Y(\%)=20.21+(0.21\pm0.02)\ln\dot{\epsilon}(ps^{-1})$ from the data shown in Fig. 4. Furthermore, the effect of experimentally realistic length of CNT's on the predicted values of ϵ_Y can be estimated from Eq. (4) as according to

$$\Delta\epsilon=-\frac{k_BT}{VK}\ln(n_{site}/n_{site}^0), \tag{6}$$

where n_{site} is linearly dependent on the length of CNT's. For a micrometer long (10,0) CNT, under the same conditions, the yield strain lowers to about $9\pm1\%$. For still longer nanotube this can lower even further. A larger diameter nanotube, of the same length, may have more activation sites n_{site} for nucleating the defects leading to the yielding of the tube. However, N, the number of single processes involved in the yielding, may also increase and offset the effect. This will not be the case if individual single-wall nanotube diameter increases by orders of magnitude, which is highly unlikely.

In Eq. (4), we note that the yield strain of CNT's is linearly dependent on the average kinetic activation energy. The static in-plane activation energy of the SW bond rotation, for several armchair and zigzag CNT's, are calculated by rotating the C-C bond in the CNT surface plane and relaxing the system at zero tension and zero temperature. The results are shown in Fig. 5. It is noticed that a small diameter zigzag nanotube has a smaller activation energy than that of a larger diameter zigzag nanotube. No such difference is obvious for the armchair nanotubes. We conducted similar MD simulations on two zigzag nanotubes (10,0) and (20,0), and two armchair nanotubes (5,5) and (10,10). The tensile yield strain of these tubes, as a function of strain rate at $T=2400$ K, is shown in Figs. 5(b) and 5(c). The pattern of static activation energy of SW rotation is clearly reflected in the corresponding yield strain. The data also suggests that the tensile yield strain can be about 2–3 % higher for large diameter tubes as compared with that of small diameter tubes under similar experimental conditions. One of the main features of the derived model is that the yield strain is strongly dependent on the activation energy. A 1 eV difference in the activation energy E_ν results in a difference of 5% in ϵ_Y. Thus, more accurate methods such as tight binding or density-functional theory under dynamic conditions are expected to further improve the above predicted yield strain of CNT's.

Above analysis shows that the yield strain of a tensile strained CNT is strongly dependent on the temperature and the applied strain rate. A physical reality that emerges from the TST based model in Eq. (4), and the MD simulation data in Fig. 4, is that the yield strains at slower strain rates and low temperatures are equivalent to the yield strains at faster strain rates and higher temperatures. From Eq. (4), this can be mathematically expressed as

$$\left(\frac{\dot{\epsilon}_1N}{n_{site}\dot{\epsilon}_0}\right)^{T_1}=\left(\frac{\dot{\epsilon}_2N}{n_{site}\dot{\epsilon}_0}\right)^{T_2}, \tag{7}$$

which shows that the yielding process can be accelerated by doing the MD simulations at higher temperatures and faster strain rates. In a different context, Voter *et al.* have used the high-temperature accelerated dynamics to study the diffusion on solid surfaces,[20] which shows that more realistic experimental deposition rates can be reproduced through this scheme.

Finally, the experiments show the tensile strength of 40–50 GPa for SWCNT ropes and MWCNT's, even though their yield strains are different: 5–6 % for SWCNT's and 12% for MWCNT's. Equation (4) shows that the yield strain ϵ_Y is a function of activation volume V and Young's modulus K as well. Since K is shown to be about 1 TPa for diverse SWCNT's and MWCNT's, the difference could be related to the activation volume. It is reasonable to expect a smaller activation volume on the outer shell of a MWCNT due to the presence of inner-shell CNT's, and the reduced V will increase the value of ϵ_Y for MWCNT's.

In summary, a transition state theory based model is developed for the yielding of CNT's. A comparison of the yield strain as a function of temperature and strain rate as derived from the model with the MD simulation results show a very good agreement between the two. Furthermore, the model predicts that a defect-free micrometer long single-wall nanotube at 300 K, stretched with a strain rate of 1%/h, yields at about $9\pm1\%$ tensile strain for small diameter CNTs and about 2–3 % higher for larger diameter CNT's. This is in good agreement with recent experimental findings.

Note added. After the completion of our original work and submission of the manuscript, we became aware of a study of static activation barrier for SW defects on CNT's, where the activation energy was calculated from bond rotation on graphene plane using Tersoff-Brenner potential. In this paper, 17% tensile strain for CNT's was estimated from a simple Arrhenius description.[21] In our work a general strain rate and temperature-dependent formula is derived, which gives tensile strain for all types of CNT's at experimentally feasible condition with dynamics activation barriers.

We thank Dr. M. Baskes and Dr. A. Voter for helpful discussions. This work is supported by NASA Contract No. NCC2-5400. D.S. was supported by NASA Contract No. 704-40-32 to CSC at Ames Research Center.

[1] S. Iijima, Nature (London) **354**, 56 (1991); **363**, 603 (1993); D.S. Bethune *et al.*, *ibid.* **363**, 605 (1993).

[2] B.I. Yakobson, M.P. Campbell, C.J. Brabec, and J. Bernholc, Comput. Mater. Sci. **8**, 341 (1997).

[3] B.I. Yakobson, Appl. Phys. Lett. **72**, 918 (1998).

[4] D.A. Walters *et al.*, Appl. Phys. Lett. **74**, 3803 (1999).

[5] M.-F. Yu, B.S. Files, S. Arepalli, and R.S. Ruoff, Phys. Rev. Lett. **84**, 5552 (2000).

[6] M.-F. Yu, O. Lourie, M.J. Dyer, K. Moloni, T.F. Kelly, and R.S. Ruoff, Science **287**, 637 (2000).

[7] P. Zhang, P.E. Lammert, and V. Crespi, Phys. Rev. Lett. **81**, 5346 (1998).

[8] M.B. Nardelli, B.I. Yakobson, and J. Berholc, Phys. Rev. Lett. **81**, 4656 (1998).
[9] Q. Zhao, M.B. Nardelli, and J. Bernholc, Phys. Rev. B **65**, 144105 (2002).
[10] D. Srivastava, M. Menon, and K. Cho, Phys. Rev. Lett. **83**, 2973 (1999).
[11] C. Wei, D. Srivastava, and K. Cho, Computer Modeling in Engineering and Sciences **3**, 255 (2002).
[12] G. Halsey, H.J. White, and H. Eyring, Text. Res. J. **15**, 295 (1945).
[13] J.C. Tully *et al.*, Phys. Rev. B **31**, 1184 (1985).
[14] J. Tersoff, Phys. Rev. B **37**, 6991 (1988).
[15] D.W. Brenner, Phys. Rev. B **42**, 9458 (1990).
[16] D. Srivastava, C. Wei, and K. Cho, Rev. Appl. Mech. **56**, No. 2 March (2003).
[17] D.H. Roberston, D.W. Brenner, and J.W. Mintmire, Phys. Rev. B **45**, 12 592 (1992).
[18] E. Hernandez *et al.*, Phys. Rev. Lett. **80**, 4502 (1998).
[19] D. Sanchez-Portal *et al.*, Phys. Rev. B **59**, 12 678 (1999).
[20] M.R. Sorensen, and A. Voter, J. Chem. Phys. **112**, 9599 (2000); F. Montaleti, M.R. Sorensen, and A. Voter, Phys. Rev. Lett. **87**, 126101 (2001).
[21] G.G. Samsonidze, G.G. Samsonidze, and B.I. Yakobson, Phys. Rev. Lett. **88**, 065501 (2002).